Journal of Electrical Engineering & Technology (2023) 18:981–989
https://doi.org/10.1007/s42835-022-01350-6

INVITED PAPER

Sensorless Control of the Switched Reluctance Motor Based on the Sliding-Mode Observer

Xinyu Li[1] · Jiayu Liu[1] · Lefei Ge[1] · Jixi Zhong[1] · Jiale Huang[1] · Yuchen Zhao[2] · Shoujun Song[1]

Received: 6 March 2022 / Revised: 5 December 2022 / Accepted: 7 December 2022 / Published online: 15 December 2022
© The Author(s) under exclusive licence to The Korean Institute of Electrical Engineers 2022

Abstract
To upgrade the application of switched reluctance motors (SRMs) for more electric aircraft, this paper presents a method with sensorless control based on the flux-linkage data from the finite element method. First, a calibration strategy is employed to obtain the flux-linkage characteristics. Then, a sliding-mode observer is used to realize the sensorless control of the SRM. The proposed method only requires the flux-linkage of the SRM at aligned and unaligned rotor positions from the experiment which takes a low-measurement effort to get the rotor position and has better accuracy in position and speed estimation than the FEM. Experimental results verify the accuracy and effectiveness of the proposed method.

Keywords Switched reluctance machine (SRM) · Sensorless control · Calibration strategy · Sliding-mode observer

1 Introduction

Switched Reluctance Machine (SRM) is a new type of motor that has attracted much attention in recent years. Due to its low cost, firm and simple structure, and wide speed range, it has broad development prospects [1]. With the continuous development of multi-electric aircraft, there is a need for more built-in starters/generators that can be used in the complex and harsh environments of the aircraft. The excellent characteristics of SRM make it an important alternative. However, due to the non-linear characteristics of the SRM, it still has a lot of problems to be solved urgently in terms of power converter design, motor design, high-performance control, and position senseless technology.

Because SRM relies on position closed-loop to drive, an accurate rotor position is required for effective control. Traditional mechanical position sensors require a large enough area for installation, which increases the volume, cost, and complexity of the motor. The photoelectric position sensor is susceptible to interference from complex conditions such as dust, which causes its accuracy to drop drastically. In this context, the position sensorless control of SRM has become an important direction of SRM research. In [2], a new method to detect the initial rotor position of SRM is presented, which doesn't need any extra premeasurement. The method of sensorless control of SRM can be classified into the following categories: observer-based methods [3, 4], magnetic characteristics-based methods [5, 6] artificial intelligence-based methods [7, 8], inductance gradient-based methods [9], and back-emf-based estimation [10]. Among these methods, observer-based methods can estimate the rotor position and speed from the known inputs. These kinds of methods are simple and robust, which are very popular in the field of machine control.

The SMO is a simple and intolerant method. There are many research advances for SMO [11]. In [12], a hybrid model is proposed, which employs two-running algorithms

✉ Lefei Ge
lge@nwpu.edu.cn

Xinyu Li
1143793425@qq.com

Jiayu Liu
2019303614@mail.nwpu.edu.cn

Jixi Zhong
zhongjx@mail.nwpu.edu.cn

Jiale Huang
huangjl@mail.nwpu.edu.cn

Yuchen Zhao
185946856@qq.com

Shoujun Song
sunnyway@nwpu.edu.cn

1 School of Automation, Northwestern Polytechnical University, Xi'an, China

2 School of Automation, Harbin University of Science and Technology, Harbin, China

of both current-based and flux-based SMO for wide-range operation. In [13], a sliding-mode observer control scheme is used to promote the UPQC's performance. The scheme considers more model uncertainties such as inductor and phase resistance. In [14], a four-quadrant operation with an SMO-based algorithm is presented. Over time, SMO has become more closely linked to other technologies. In [15], Back-propagation (BP) neural network with a phase-locked loop (PLL) is used in an SMO to estimate the speed and position of permanent magnet synchronous motors (PMSMs). The accuracy is greatly improved. Ningning Ren's study shows that SMO based on sigmoid function has high precision and avoids chattering under different conditions [16]. The features of both the exponential reaching law (ERL) and the power rate reaching law (PRL) also can be integrated into the design of the SMO to optimize the result of estimation [17]. The flux-model-based SMO is presented in [18], and this model uses magnetizing curves and assumes the monotonically increasing function for flux-linkage. In [19], a flux-model-based SMO is used and flux-excitation-position data is adopted to develop a Fourier expression for flux-linkage. Therefore, the error in the flux measurement might influence the error in rotor position estimation.

Various studies have been carried out to reduce errors in flux estimation for sensorless control of the SRM [20]. An automated winding resistance correction method is used to correct a circuit-based flux-linkage measurement method. Although this can reduce and eliminate errors, it requires additional circuit components [21]. An inductance model based on the SMO is used to reduce the requirement of additional functions for flux-linkage calculation and the model only uses operating signals [22]. To reduce the complexity of the analytical expression, a transformed saturated inductance characteristics-based method is proposed [23]. In [24], an integral flux error correction technique is designed to reduce phase resistance error caused by temperature variation. A third-order phase-licked loop is applied to reduce the effect of SRM terminal measurement noise and numerical measurement residual error caused by a numerical method of flux estimation [25].

This paper presents an accurate sensorless control method based on the calibrated flux-linkage characteristics and the SMO which has more appropriate gains. The contributions of this paper can be concluded as follows.

(1) The proposed method only requires the flux-linkage of the SRM at aligned and unaligned rotor positions from the experiment, which takes a low-measurement effort to get the rotor position. The calibration method can improve the accuracy of the flux-linkage characteristics significantly. Meantime, the selection of the SMO parameters also improves the dynamic performance of the estimation.

(2) Using better flux-linkage characteristics, can get better current results through the look-up table. The estimation of the speed and position is extremely relevant to the precision of the flux-linkage characteristics. Compared to the FEM simulations, the proposed method is robust to parameter variations and has better accuracy in position and speed estimation.

(3) The experiment shows the estimated results of the speed and position. The proposed method demonstrates a high degree of accuracy and dynamic response. In a wide variable speed range, the proposed method can still maintain high accuracy and good tracking performance.

2 Reluctance Calibration Strategy

The reluctance calibration strategy is based on the flux-linkage characteristics obtained by the indirect method and FEM. Using the reluctance calibration strategy can effectively boost the precision of the flux-linkage characteristics. In this section, a reluctance calibration strategy is introduced to calibrate the results from FEM simulation and the indirect method without a rotor clamping device [26].

2.1 Measurement of Flux-Linkage Characteristics

Among all the flux-linkage characteristics, flux characteristics at aligned and unaligned positions are the most important. To obtain the flux-linkage characteristics of SRM, the first step is to measure the flux-linkage at aligned and unaligned positions.

According to [27], an indirect method to measure flux-linkage at aligned positions is presented. The flux-linkage at an unaligned position can be obtained by calculating the unaligned inductance from the dynamic current waveform.

The phase voltage equation of an SRM can be written as

$$u = Ri + L\frac{di}{dt} + i\omega\frac{dL}{d\theta} \tag{1}$$

where i is the phase current, L is the phase inductance and ω and θ are the machine rotor angular speed and position, respectively.

The back electromotive ($i\omega dL/d\theta$) can be eliminated at an unaligned position and low speed. Hence, the inductance at an unaligned position can be deducted as

$$L = \frac{u - Ri}{di/dt} \tag{2}$$

The current change rate can be estimated with the least-squares method (LSM) as

$$\frac{di}{dt}=\frac{\sum_{k=1}^{n}\left(t_{\mathrm{k}}-\frac{1}{n}\sum_{k=1}^{n}t_{\mathrm{k}}\right)\left(i_{\mathrm{k}}-\frac{1}{n}\sum_{k=1}^{n}i_{\mathrm{k}}\right)}{\sum_{k=1}^{n}\left(t_{\mathrm{k}}-\frac{1}{n}\sum_{k=1}^{n}t_{\mathrm{k}}\right)^{2}} \tag{3}$$

where t_k and i_k are the instantaneous time and current, respectively, and n is the number of samples.

Based on the curve-fitting result with the LSM, the flux-linkage trajectory at the unaligned position can be calculated.

2.2 Reluctance Calibration Strategy

According to MEC, the reluctance can be obtained from flux-linkage characteristics, which is given as

$$R=\frac{\theta}{\phi}=\frac{N^2 I}{\psi} \tag{4}$$

where N is the number of turns, ϕ is magnetic flux, and ψ is the phase flux linkage, respectively.

The reluctance of the SRM consists of airgap reluctance and iron core reluctance. The airgap reluctance R_g can be calculated from the airgap inductance L_g as

$$R_g=\frac{N^2}{L_g}=\frac{l_g}{\mu_0 S} \tag{5}$$

where l_g, μ_0, and S are the mean effective length of airgap, the air magnetic permeability, and the cross-sectional area of airgap, respectively.

In Fig. 1, θ_u is the unaligned position, θ_a is the aligned position, θ_1 is the position where the rotor pole and the stator pole begin to overlap, θ_2 is the position where the back edge of the rotor pole and stator pole begin to overlap.

The air gap inductance is a nonlinear function of rotor position θ. The measured airgap reluctance at unaligned and aligned positions are used to calibrate the reluctance in these two regions.

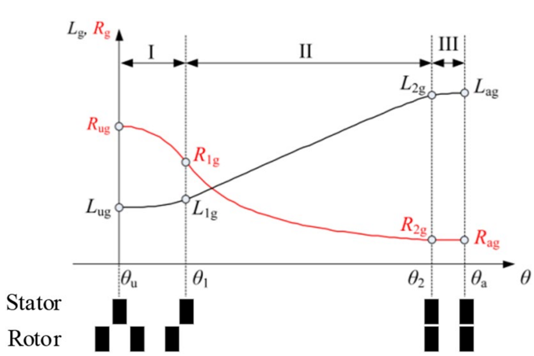

Fig.1 Airgap inductance and reluctance with the function of rotor position

$$R_{\mathrm{g,Cali.}}(\theta)=\frac{R_{\mathrm{ug,Mea.}}}{R_{\mathrm{ug,Sim.}}}R_{\mathrm{g,Sim.}},\theta_{\mathrm{u}}\le\theta\le\theta_1 \tag{6}$$

$$R_{\mathrm{g,Cali.}}(\theta)=\frac{R_{\mathrm{ag,Mea.}}}{R_{\mathrm{ag,Sim.}}}R_{\mathrm{g,Sim.}},\theta_2\le\theta\le\theta_{\mathrm{a}} \tag{7}$$

where $R_{\mathrm{g,\ Sim.}}$, $R_{\mathrm{g,\ Mea.}}$, and $R_{\mathrm{g,\ Cali.}}$ are FEM simulated, measured, and calibrated reluctance, respectively. $R_{\mathrm{ug,Mea.}}$, $R_{\mathrm{ug,Sim.}}$, $R_{\mathrm{ag,Mea.}}$ and $R_{\mathrm{ag,Sim.}}$ are the corresponding values at θ_u and θ_a, respectively.

Iron core reluctance R_i can be calculated as

$$R_i=\frac{l_i}{\mu_0\mu_r S} \tag{8}$$

where l_i andμ_r are average flux paths in the ferromagnetic material and relative permeability of ferromagnetic material, respectively.

At first, μ_r is assumed to be independent with the rotor position, and it only depends on the phase current, it is calibrated as

$$\mu_{\mathrm{r,Cali}}=\frac{R_{\mathrm{ai,Sim}}}{R_{\mathrm{ai,Mea}}}\mu_{\mathrm{r}} \tag{9}$$

The simulated iron reluctance can be calibrated

$$R_{\mathrm{i,Cali}}(\theta)=\frac{\mu_{\mathrm{r}}}{\mu_{\mathrm{r,Cali}}}R_{\mathrm{i,Sim}}(\theta)=\frac{R_{\mathrm{ai,Mea}}}{R_{\mathrm{ai,Sim}}}R_{\mathrm{i,Sim}}(\theta) \tag{10}$$

The total calibrated reluctance is the sum of the calibrated airgap and iron core reluctance, which is shown as

$$R_{\mathrm{Cali}}=R_{\mathrm{g,Cali}}+R_{\mathrm{i,Cali}} \tag{11}$$

The final calibrated flux linkage can be calculated by

$$\psi_{\mathrm{Cali}}=R_{\mathrm{g,Cali}}+R_{\mathrm{i,Cali}} \tag{12}$$

3 Sliding-Mode Observer

3.1 1Modeling of SRM

The nonlinear model of SRM can be described by

$$\frac{d\psi_{\mathrm{n}}}{dx}=v_{\mathrm{n}}(t)-i_{\mathrm{n}}(t)R_{\mathrm{n}},n=1,2,\ldots,N_{\mathrm{ph}} \tag{13}$$

where v_n and i_n are the phase voltage and current respectively, R_n is the winding resistance of active phase n, and N_{ph} is the number of phases. ψ_n is the flux-linkage, which is a nonlinear function of current and position.

The movement equations are presented in (14) and (15).

$$\frac{d\theta(t)}{dt} = \omega(t) \tag{14}$$

$$\frac{d\omega(t)}{dt} = \alpha(t) \tag{15}$$

where θ and ω are the rotor position and speed, respectively, and α is the angular speed acceleration.

3.2 SMO for SRM

The flux-linkage estimation error e_n can be defined as

$$e_n = \psi_n(t) - \psi_n'(t), n = 1, 2, 3 \tag{16}$$

where ψ_n(t) and ψ'_n(t) are measured flux-linkage and estimated flux-linkage, respectively.

Flux-linkage measurements and estimates are obtained by

$$\psi_n(t) = \int_0^t \left(v_n(\varepsilon) - i_n(\varepsilon)R_n\right)d\varepsilon \tag{17}$$

$$\psi_n'(t) = \psi_n'\left(i_n(t), \theta'(t)\right) \tag{18}$$

where v_n and i_n are phase voltage and phase current, respectively, and $\theta'(t)$ is the estimated rotor position.

To realize the closed-position control of SRM, the sliding-mode observer is required to observe and obtain the estimated rotor position and speed of the SRM. The following equations are the design principles of the sliding-mode observer

$$\begin{cases} \frac{d\theta'}{dt} = \omega' + k_\theta \mathrm{sgn}\left(e_\theta\right) \\ \frac{d\omega'}{dt} = -\frac{B}{J}\omega' + \frac{1}{J}\left(T_e' - T_L\right) + k_\omega \mathrm{sgn}\left(e_\omega\right) \\ T_e = \sum_{j=1}^{N_{ph}} \frac{1}{2}\frac{\partial L_{ph,j}}{\partial\theta} i_{ph,j}^2 \end{cases} \tag{19}$$

where *sgn*() is the sign function, e_θ and e_ω are the angle error function and speed error function, respectively. k_θ and k_ω are SMO gains. ω' is the estimated result of speed, B is the coefficient of viscosity, J is the rotary inertia, T_e and T'_e are the electromagnetic torque and the estimated electromagnetic torque, respectively. T_L is the load torque, N_{ph} is the phase number, j is the serial number from 1 to N_{ph}, $L_{ph,j}$ is the phase inductance at phase j, and $i_{ph,j}$ is the phase current at phase j.

Sliding-mode surface is defined as

$$s_\theta = e_\theta = \theta - \theta' \tag{20}$$

$$s_\omega = e_\omega = \omega - \omega' \tag{21}$$

SMO can be designed by

$$\begin{cases} \dot{\theta}' = \omega' + k_\theta \mathrm{sgn}(s) \\ \omega' = \dot{\alpha}'(t) + k_\omega \mathrm{sgn}(s) \\ \dot{\alpha}'(t) = k_\alpha \mathrm{sgn}(s) \end{cases} \tag{22}$$

where α is acceleration.

While SMO is working, the actual rotor position and speed in real-time cannot be entered directly into the SMO. The above equations cannot be calculated without the data of rotor position and speed. According to the electromagnetic torque equation, this paper chooses a new error function e_f

$$e_f = T_e - T_e' = \sum_{j=1}^{N_{ph}} \left(\frac{1}{2}\frac{\partial L_j}{\partial\theta} i_j^2 - \frac{1}{2}\frac{\partial L_j}{\partial\theta'} i_j'^2\right) \tag{23}$$

In this equation, can consider $\frac{\partial L_j}{\partial\theta} \approx \frac{\partial L_j}{\partial\theta'}$, and the value of the sign function is determined by the positive and negative of the error function. So (17) can be simplified, which is given as

$$e_f = \sum_{j=1}^{N_{ph}} \frac{1}{2}\frac{\partial L_j}{\partial\theta'}(i_j^2 - i_j'^2) \tag{24}$$

$$H_j(\theta) = \sin\left(N_r\theta - (j-1) \times \left(2\pi/N_{ph}\right)\right) \tag{25}$$

3.3 Design Gains of SMO

When SMO works, jitter is inevitable. To reduce the impact of jitter, this paper uses the following two methods.

(a) The switching surface of SMO is improved. Assuming that the linear region in the switching surface is μ, then (22) can be improved, which is given as

$$\begin{cases} \dot{\theta}' = \omega' + k_\theta \mathrm{sat}(s) \\ \omega' = \dot{\alpha}'(t) + k_\omega \mathrm{sat}(s) \\ \dot{\alpha}'(t) = k_\alpha \mathrm{sat}(s) \end{cases} \tag{26}$$

where sat() is

$$\mathrm{sat}(s) = \begin{cases} \mathrm{sgn}(s), |s| > \mu \\ s/\mu, |s| \le \mu \end{cases} \tag{27}$$

By adjusting the switching surface, the accuracy and robustness of SMO can be effectively improved.

(b) To improve the performance of the SMO, it is necessary to select an appropriate gain during design.

The estimation error of SMO is defined as follows

$$\begin{cases} e_\theta(t) = \theta(t) - \theta'(t) \\ e_\omega(t) = \omega(t) - \omega'(t) \\ e_\alpha(t) = \alpha(t) - \alpha'(t) \end{cases} \tag{28}$$

The dynamic process of error can be obtained by differentiation

$$\begin{aligned} \dot{e}_\theta &= \dot{\theta} - \dot{\theta}' = e_\omega - k_\theta \operatorname{sgn}(s) \\ \dot{e}_\omega &= \dot{\omega} - \dot{\omega}' = e_\alpha - k_\omega \operatorname{sgn}(s) \\ \dot{e}_\alpha &= \dot{\alpha} - \dot{\alpha}' = \dot{\alpha} - e_\alpha \operatorname{sgn}(s) \end{aligned} \tag{29}$$

Based on Lyapunov function

$$V = \frac{e_\theta^2}{2} \tag{30}$$

Further derivation can be obtained

$$\dot{V} = e_\theta e_\omega - e_\theta k_\theta \operatorname{sgn}(s) \tag{31}$$

To ensure that the Lyapunov dynamic function is negative at all times, it needs to satisfy

$$k_\theta > \left| e_\omega \right| \tag{32}$$

$$k_\theta > \left| e_\omega \right|_{\max} \tag{33}$$

In the case that the rotor speed cannot be measured directly, it is necessary to assume a maximum rotor speed error to ensure that the Lyapunov function meets the above conditions at any moment when the SRM is running. Therefore, the following formulas need to be met.

$$\begin{cases} k_\theta > \left| e_\omega \right|_{\max} \\ k_\omega \geq k_\theta \dfrac{\left| e_\alpha \right|_{\max}}{\left| e_\omega \right|_{\max}} \\ k_\alpha \geq k_\omega \dfrac{\left| \dot{\alpha} \right|_{\max}}{\left| e_\alpha \right|_{\max}} \end{cases} \tag{34}$$

Through all the above calculations, this paper gets the minimum gains when designing SMO and the relationship between them. By reasonably setting the maximum speed estimation error, the maximum acceleration estimation error, and the maximum acceleration change rate over time, the minimum gain can be obtained.

4 Simulation Verification

4.1 The Structure of the Control System

The proposed SMO method to estimate rotor position and speed is applied on a 12/8 three-phase SRM in MATLAB/Simulink environment. Figure 2 shows the structure of the control system based on SMO. In the simulation, the load can be adjusted to control the speed of the SRM (Fig. 3, Table 1).

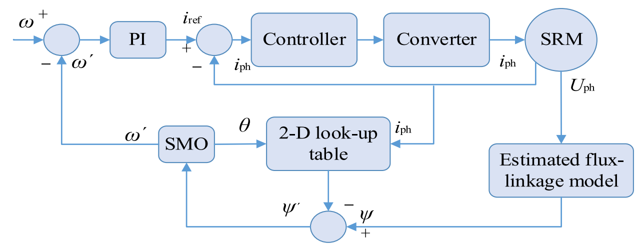

Fig.2 The control structure of SRM is based on SMO

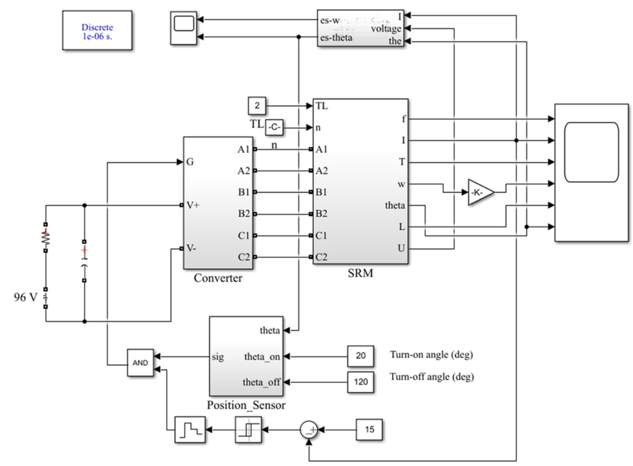

Fig.3 The simulation model of SRD

Table 1 Observer gains

k_θ	1/48
k_ω	20,000
k_α	600,000

Table 2 The main parameters of the prototype

Stator pole number	12
Rotor pole number	8
Rated power	1 kW
Rated voltage	96 V
Rated current	15 A
Rated torque	5 Nm

4.2 Build the Simulation Model

The main parameters of the prototype are shown in Table 2.

Based on the principles introduced before, the SMO simulation model is built.

To control the SRM in a wide range of speeds, and ensure the rapid response of the motor at different rated speeds. A look-up table in the first integral part is added. The look-up table reflects the difference of the initial value in the integral part at different speed ranges.

4.3 Simulation Results

The simulations are performed at 1000–1500 rpm at 5 Nm to verify the effectiveness and accuracy of the proposed method (Fig. 4). The simulation results are shown in Figs. 5, 6 and 7.

To prove that the flux-linkage characteristics obtained after the reluctance calibration method are applied in the sliding-mode observer, the estimation accuracy can be significantly improved, this paper also simulates by using the flux-linkage characteristics obtained by FEM (Table 3).

Figure 4 shows the estimated position and actual position at steady-state and Fig. 5 shows the comparison of the reluctance calibration method and finite element method. Figure 6 shows the comparison of the reluctance calibration method and finite element method when rotor speed from 1000 to 1500 rpm.

Simulation results demonstrate the effectiveness of the SMO method to estimate the position and speed at high-speed operation. The speed errors are calculated and shown in Table 4.

The estimated error of speed and position is mainly caused by the errors generated when estimating the flux linkage. As shown in Figs. 5 and 6, using the FEM to obtain the flux linkage cannot always get a good result in position and speed estimation. Using calibration method to calibrate the FEM results, can further validate the effectiveness and applicability.

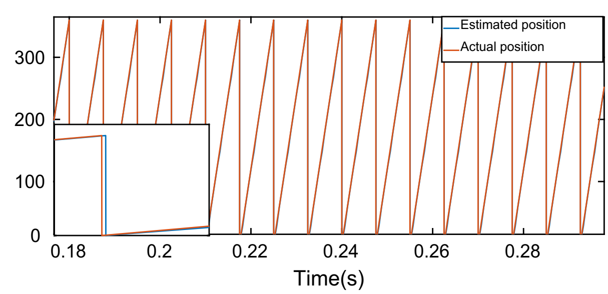

(a) Reluctance calibration

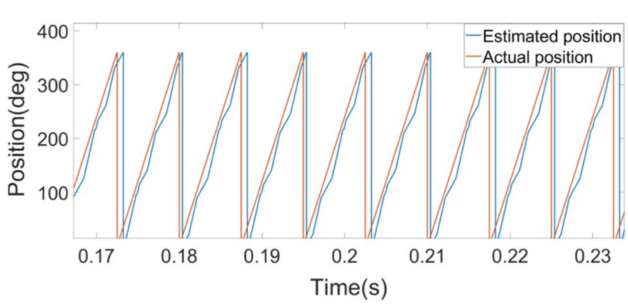

(b) FEM

Fig.4 Simulation results of the rotor position estimation at 1000 rpm

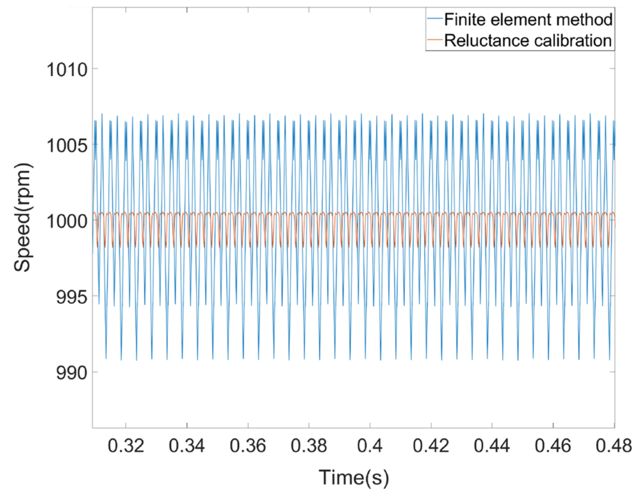

(a) 1000 rpm

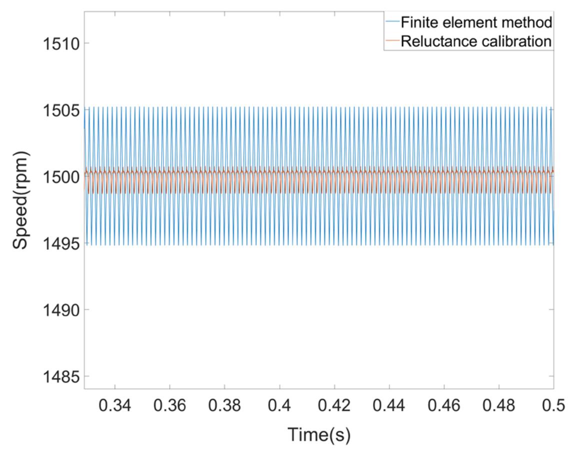

(b) 1500rpm

Fig.5 Simulation results of the rotor speed estimation

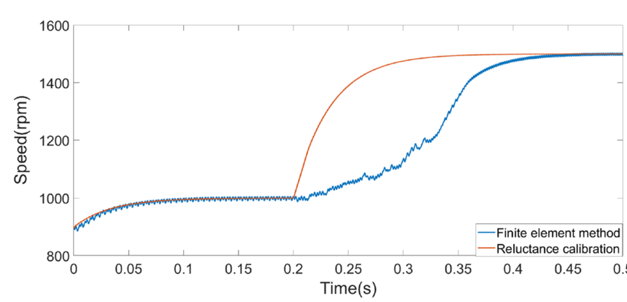

Fig.6 Simulation results of the rotor speed estimation from 1000 to 1500 rpm

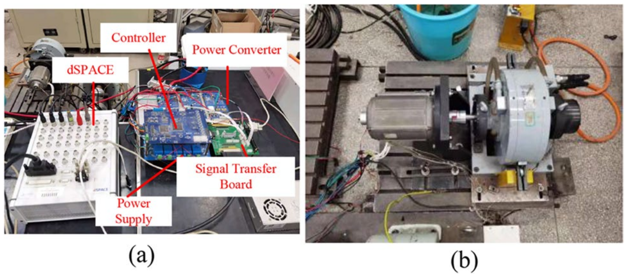

Fig. 7 Experimental setup

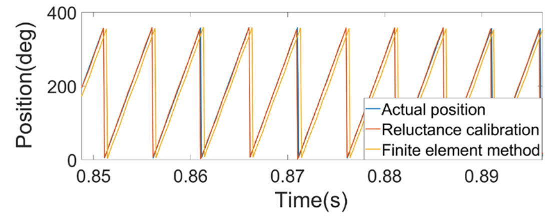

Fig. 8 Experimental results of the rotor position estimation at 1500 rpm

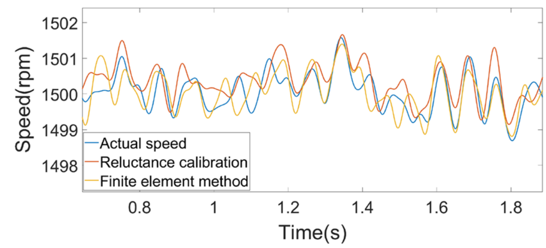

Fig. 9 Experimental results of the rotor speed estimation at 1000 rpm

Table 3 The position estimation error

Methods	MAE	RMSE
Reluctance calibration	0.17°	0.20°
FEM	1.10°	1.32°

Table 4 The speed errors

Speed	Reluctance calibration (%)	FEM (%)
1000 rpm	0.52	0.95
1500 rpm	0.23	0.36

From the error calculation and comparison of the table above, it can be seen that

(a) The estimation error of the SMO in the wide speed range is very small and fully conforms to the design requirements, and the flux-linkage characteristics obtained by the reluctance calibration method are more accurate.
(b) The estimation error of the slide observer decrease in multiples and the fluctuation decreases significantly.

5 Experimental Verification

A semi-physical simulation development platform consisting of an SRM peripheral hardware platform and a dSPACE system was built. Due to the limitation of the experimental test bench, the experiments are performed when the load torque is set to 2Nm in Figs. 8, 9 and 11. In the case of load change, the torque varies from 2 to 1 Nm in Fig. 10 (Table 5).

The experiment result of rotor position estimation is shown in Fig. 8. The actual position measured by the resolver is recorded for comparison. Figure 9 shows the experimental result of the estimated rotor speed. Figure 10 shows that the estimated rotor speed can track the actual rotor speed perfectly when torque is changing. Figure 11 shows the calibration method can work in a wide speed arrange and

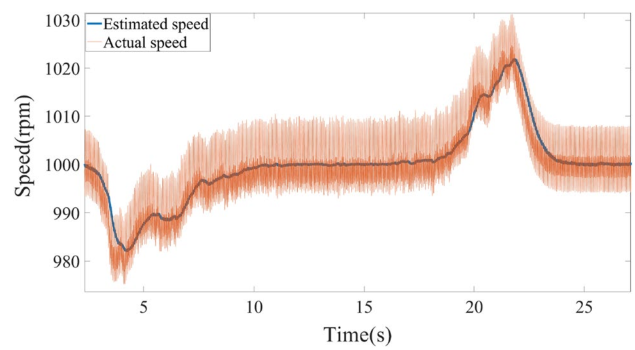

Fig. 10 Experimental results of the rotor speed estimation at 1000 rpm when torque is changing from 2 to 1 Nm

Table 5 The position estimation error

Speed	MAE	RMSE
1500 rpm	0.54°	0.65°

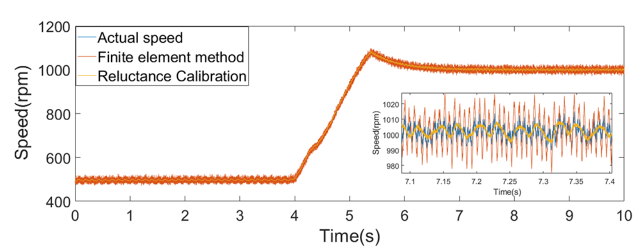

Fig. 11 Experimental results of the rotor speed estimation from 500 to 1000 rpm

has a high dynamic response. When the speed varies from 500 to 1000 rpm, the estimated position and speed can track the actual position and speed precisely. The speed error is between 0.5 and 4%. The SMO is usually performing better in high speed, so the error is large at low speed. However, the proposed method can work in a wide speed range and show good precision and track performance. The reluctance calibration method can calibrate the FEM simulation results and apply them in the experiment. The result shows that this calibration method has certain robustness and precision to the variation of experiment parameters.

During the experiment, the motor working conditions under different speeds and load conditions were verified, the motor runs smoothly, and realizes the sensorless control of the motor very well.

The experimental results are different from the previous simulation results, which is mainly due to the vibration, electromagnetic interference, and other interference factors in the experimental process. These factors have a greater impact on the actual operation of the SRM. However, from the overall law of the experiment, it is still consistent with the previous theoretical simulation.

From the experimental results, this paper proves that the rotor position and speed can be precisely estimated with an acceptable error. It demonstrates that the proposed method can be applied for SRM sensorless control.

6 Conclusion

This paper proposes a new sensorless control method for SRM drives based on SMO. A reluctance calibration method is introduced to improve the finite element simulation results. It can effectively obtain the flux linkage characteristics of the SRM on the standard test bench and has a certain degree of robustness to parameter variations. In addition to geometric characteristics, only the rotor positions at aligned and non-aligned positions that are convenient for measurement need to be obtained. Compared to traditional methods, such as the FEM method, the method is simple, fast, and accurate, does not require a special test bench, reduces the cost and complexity, is convenient, and is suitable for practical applications. This paper estimates the current based on the flux linkage and rotor position of SRM. Based on the estimated and actual current, the sliding-mode surface in the SMO design is formed. To ensure the accuracy and stability of the SMO work, this paper completes the SMO design by the calculation and selection of the optimal gain values. Through simulation and experiment, this paper proves that the calibration strategy can be used in the current estimation for the SMO to improve the dynamic response and estimation accuracy.

Acknowledgements This work was supported in part by National Natural Science Foundation of China under Grant 52107055, in part by Key Research and Development Program of Shaanxi Province under Grant 2022GY-260, in part by China Postdoctoral Science Foundation under Grant 2021M691996, in part by Fundamental Research Funds for the Central Universities 3102021ZDHQD03, and in part by National Natural Science Foundation of China under Grant 51877179.

References

1. Borg Bartolo J, Degano M, Espina J, Gerada C (2017) Design and initial testing of a high-speed 45-kW switched reluctance drive for aerospace application. IEEE Trans Ind Electron 64(2):988–997
2. Ge L, Xu H, Guo Z, Song S, De Doncker RW (2021) An optimization-based initial position estimation method for switched reluctance machines. IEEE Trans Power Electron 36(11):13285–13292
3. Sun J, Cao G, Huang S, Peng Y, He J, Qian Q (2019) Sliding-mode observer-based position estimation for sensorless control of the planar switched reluctance motor. IEEE Access 7:61034–61045
4. Nakazawa Y, Matsunaga S (2019) Position sensorless control of switched reluctance motor using state observer. In: 22nd international conference on electrical machines and systems (ICEMS), Harbin, China, pp 1–4
5. Liang Y, Chen H (2018) Circuit-based flux linkage measurement method with the automated resistance correction for SRM sensorless position control. IET Electr Power Appl 12(9):1396–1406
6. Zhang L, Liu C (2020) A sensorless techniques for switched reluctance motor considering mutual inductances. In: IEEE 5th information technology and mechatronics engineering conference (ITOEC), Chongqing, China, pp 1425–1428
7. Cai Y, Wang Y, Xu H, Sun S, Wang C, Sun L (2018) Research on rotor position model for switched reluctance motor using neural network. IEEE/ASME Trans Mechatron 23(6):2762–2773
8. Hassoun Y, Rifai MB (2017) Drive of senseless Switched Reluctance Motor (SRM) depending on Artificial Neural Networks. In: 10th Jordanian international electrical and electronics engineering conference (JIEEEC), Amman, pp 1–9
9. Shao J, Deng Z, Gu Y (2016) Sensorless control for switched reluctance motor based on gradient of phase inductance. Electron Lett 52(19):1600–1601
10. Tang Y, He Y, Wang F, Lee D, Ahn J, Kennel R (2018) Back-EMF based sensorless control system of hybrid SRM for high-speed operation. IET Electr Power Appl 12(6):867–873
11. Wang X, Peng F, Emadi A (2016) A position sensorless control of switched reluctance motors based on sliding-mode observer. In: 2016 IEEE Transportation Electrification Conference and Expo (ITEC) pp. 1–6
12. Divandari M, Koochaki A, Jazaeri M, Rastegar H (2007) A novel sensorless SRM drive via hybrid observer of current sliding mode and flux linkage. In: 2007 IEEE international electric machines & drives conference, Antalya, pp 45–49
13. Heidari MA, Nafar M, Niknam T (2022) A novel sliding mode based UPQC controller for power quality improvement in micro-grids. J Electr Eng Technol 17:167–177
14. Khalil A, Underwood S, Husain I, Klode H, Lequesne B, Gopala Krishnan S, Omekanda AM (2007) Four-quadrant pulse injection and sliding-mode-observer-based sensorless operation of a switched reluctance machine over entire speed range including zero speed. IEEE Trans Ind Appl 43(3):714–723
15. Wang G, Zhang H (2022) A second-order sliding mode observer optimized by neural network for speed and position estimation of PMSMs. J Electr Eng Technol 17:415–423

16. Ren N, Fan L, Zhang Z (2021) Sensorless PMSM control with sliding mode observer based on sigmoid function. J Electr Eng Technol 16:933–939
17. Brahmi B, Bojairami IE, Saad M et al (2021) Enhancement of sliding mode control performance for perturbed and unperturbed nonlinear systems: theory and experimentation on rehabilitation robot. J Electr Eng Technol 16:599–616
18. Islam MS, Husain I, Veillette RJ, Batur C (2003) Design and performance analysis of sliding-mode observers for sensorless operation of switched reluctance motors. IEEE Trans Control Syst Technol 11(3):383–389
19. Li P, Zhang L, Yu Y (2017) A novel sensorless for switched reluctance motor based on sliding mode observer. In: IEEE 2nd advanced information technology, electronic and automation control conference (IAEAC), Chongqing, pp 1560–1564
20. Ge L, Burkhart B, De Doncker RW (2020) Fast iron loss and thermal prediction method for power density and efficiency improvement in switched reluctance machines. IEEE transactions on industrial electronics 67(6):4463–4473
21. Liang Y, Chen H (2018) Circuit-based flux linkage measurement method with the automated resistance correction for SRM sensorless position control. IET Electr Power Appl 12(9):1396–1406
22. Dankadai NK, Elgendy MA, Mcdonald SP, Atkinson DJ, Atkinson G (2019) Assessment of sliding mode observer in sensorless control of switched reluctance motors. In: 2019 IEEE 13th international conference on power electronics and drive systems (PEDS), pp 1–6
23. Ge L, Zhong J, Bao C, Song S, De Doncker RW (2022) Continuous rotor position estimation for SRM based on transformed unsaturated inductance characteristic. IEEE Trans Power Electron 37(1):37–41
24. Wei W, Wang Q, Nie R (2017) Sensorless control of double-sided linear switched reluctance motor based on simplified flux linkage method. CES Trans Electr Mach Syst 1(3):246–253
25. Peng F, Ye J, Emadi A (2016) Position sensorless control of switched reluctance motor based on numerical method. In: 2016 IEEE energy conversion congress and exposition (ECCE) pp 1–8
26. Ge L, Ralev I, Klein-Hessling A, Song S, De Doncker RW (2020) A simple reluctance calibration strategy to obtain the flux-linkage characteristics of switched reluctance machines. IEEE Trans Power Electron 35(3):2787–2798
27. Hofmann A, Klein-Hessling A, Ralev I, De Doncker RW (2015) Measuring SRM profiles including radial force on a standard drives test bench. In: Proceedings of international electric machines & drives conference, May 2015, pp 383–390

Publisher's Note Springer Nature remains neutral with regard to jurisdictional claims in published maps and institutional affiliations.

Springer Nature or its licensor (e.g. a society or other partner) holds exclusive rights to this article under a publishing agreement with the author(s) or other rightsholder(s); author self-archiving of the accepted manuscript version of this article is solely governed by the terms of such publishing agreement and applicable law.

Xinyu Li He received B.S. degree from Northwestern Polytechnical University, Xi'an, China, in 2021, where he is currently working toward the M.S. degree. His research interests include electrical machines and drives with emphasis on switched reluctance machines and aircraft starter/generator.

Jiayu Liu She is enrolled in 2019 and is currently an undergraduate student at Northwestern Polytechnical Polytechnical University, Xi'an, China, majoring in electrical engineering and its automation, with research interests in areas such as switched reluctance motor.

Lefei Ge (Member, IEEE) He received the B.S. degree in measurement and control technology and the M.S. degree in electrical engineering from Northwestern Polytechnical University, Xi'an, China, in 2013 and 2016, respectively, and the DR.-Ing. degree in electrical engineering from RWTH Aachen University, Aachen, Germany, in 2020. In September 2016, he became a Research Associate with the Institute of Power Electronics and Electrical Drives, RWTH Aachen University. Since 2020, he has been an Associate Professor with the Department of Electrical Engineering, Northwestern Polytechnical University. His research interests include electrical machines and drives with emphasis on switched reluctance machines.

Jixi Zhong He received the B.S. degree in electrical engineering from Northwestern Polytechnical University, Xi'an, China, in 2020, where he is currently pursuing the M.S. degree in electrical engineering. His research interests include electrical machines and drives with emphasis on the advanced control of switched reluctance machines.

Jiale Huang He received the B.S. degree in electrical engineering from Northwestern Polytechnical University, Xi'an, China, in 2021, where he is currently pursuing the M.S. degree in power energy. His research interests include design and control of switched reluctance machines.

Yuchen Zhao He is enrolled in 2020 and is currently an undergraduate student at Harbin University of Science And Technology, Harbin, China, majoring in electrical engineering and its automation, with research interests in areas such as PMSM and SRM.

Shoujun Song (Senior Member, IEEE) He received the B.S. and M.S. degrees from Northwestern Polytechnical University, Xi'an, China, in 2003 and 2006, respectively, and the Dr.-Ing. degree from the Technical University of Berlin, Berlin, Germany, in 2009, all in electrical engineering. He is currently a Professor with the Department of Electrical Engineering, Northwestern Polytechnical University. His research interests include electrical machines and drives with emphasis on switched reluctance machines and permanent magnet machines.